Performance Derating of Multi-Three-Phase PM-Assisted Synchronous Reluctance Motors in Open-Three-Phase Fault Condition

# Performance Derating of Multi-Three-Phase PM-Assisted Synchronous Reluctance Motors in Open-Three-Phase Fault Condition

Simone Ferrari
*Energy Department "Galileo Ferraris"*
*Politecnico di Torino*
Turin, Italy
simone.ferrari@polito.it

Sandro Rubino
*Energy Department "Galileo Ferraris"*
*Politecnico di Torino*
Turin, Italy
sandro.rubino@polito.it

Fabio Mandrile
*Energy Department "Galileo Ferraris"*
*Politecnico di Torino*
Turin, Italy
fabio.mandrile@polito.it

Andrei Bojoi
*Energy Department "Galileo Ferraris"*
*Politecnico di Torino*
Turin, Italy
andrei.bojoi@polito.it

Eric Armando
*Energy Department "Galileo Ferraris"*
*Politecnico di Torino*
Turin, Italy
eric.armando@polito.it

Gianmario Pellegrino
*Energy Department "Galileo Ferraris"*
*Politecnico di Torino*
Turin, Italy
gianmario.pellegrino@polito.it

***Abstract*—Multi-three-phase (M3PH) motor drives are experiencing increasing development in safety-critical applications since they can be configured as multiple three-phase conversion units operating in parallel, guaranteeing modular fault tolerance after an open-three-phase fault. Although most literature on M3PH applications considers induction or surface-mount permanent magnet (PM) motors, the development of interior PM (IPM) machines has gained more attention in recent years. Indeed, requirements like a wide constant power speed range, high power density and efficiency are now considered mandatory for propulsion applications. In this scenario, PM-assisted synchronous reluctance (PM-SyR) motors represent a key compromise among the potential IPM configurations as they satisfy the requirements above and minimize PM utilization. Currently, literature contributions are missing investigating the performance derating of M3PH PM-SyR motors in open-three-phase fault conditions. Therefore, this paper proposes a performance derating analysis of a 60 kW prototype by considering performance indicators like efficiency, torque ripple, power factor, and maximum torque per speed capability.**

***Index Terms*—Multi-Three-Phase Machines, Electrical Machines, Interior Permanent Magnet Synchronous Machine.**

## I. Introduction

Multi-three-phase (M3PH) motors are receiving significant attention in safety-critical applications since these multiphase solutions allow three-phase drive modularity [1]–[3]. Indeed, the machine stator consists of independent three-phase windings with isolated neutral points fed by three-phase inverters. This way, the consolidated three-phase technologies can be used, significantly reducing costs and design time. Moreover, M3PH drives allow for extending the three-phase modularity in terms of fault tolerance, allowing a straightforward post-fault drive configuration. Indeed, in the case of an open-phase fault, the faulted three-phase unit (motor windings plus inverter) is simply disconnected from the DC supply.

Considering M3PH motor solutions, most literature focuses on the optimal design of induction or surface-mount permanent magnet (PM) motors. Indeed, these solutions are the most employed in safety-critical propulsion applications like surface vessels or aerospace [4]–[7]. However, in the wake of recent developments in traction applications [8], new M3PH drives are now required to operate in a wide constant power speed range by exhibiting high efficiency and torque density, which are assumed to be mandatory key performance indicators. Interior PM (IPM) motors currently represent a straightforward solution that satisfies these requirements [9]. However, the recent need to reduce rare earth PM utilization makes PM-assisted synchronous reluctance (PM-SyR) motors one of the more competitive among IPM configurations. Indeed, torque production of PM-SyR motors is obtained mainly through magnetic reluctance, while PMs are just used to increase the overall power factor to get a wide constant power speed range.

Although PM-SyR motors may represent the future state-of-art for M3PH drives, the literature does not report a dedicated analysis of their performance derating following an open-three-phase fault event. This analysis is even more justified in M3PH motors having many three-phase units, which can operate in severe fault conditions, i.e., loss of a significant number of three-phase units (two or more). According to this outlook, this paper evaluates the derating of the leading performance indicators of M3PH PM-SyR motors operating in severe open three-phase fault conditions, considering both fundamental and harmonic-related indexes. As a case example, the proposed analysis considers a 12-phase PM-SyR prototype using a quadruple-three-phase asymmetrical stator winding configuration. Its cross section is reported in Fig. 1, while its ratings are listed in Tab. I. The motor is equipped with a asymmetric 4x3 phase winding, with full pitch. The selected

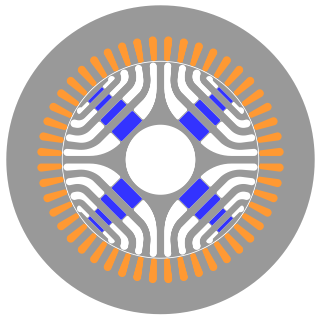

Fig. 1. Cross-section of the PM-SyR machine selected as benchmark.

design adopts NdFeB PMs (N33SH) that, together with the magnetic design push the demagnetization limit at safe levels.

The analysis is performed using SyR-e [10], that is improved to cover also N3PH machines and perform the analysis presented in the following. In the study, four derating scenarios will be considered, ranging from the less severe (1 of 4 sets off) to the most severe (3 of 4 sets off), considering all the possible combinations. The healthy scenario (all the 4 sets on) will be also included in the comparison as a reference.

The paper is organized as follow: Sec. II will focus on modeling of M3PH motor drives, giving the theoretical background needed for the next steps. Sec. III will compare all the possible derating in terms of magnetic model of the motor, considering the whole current domain and giving details on some selected operating points, to better understand the differences between derating scenarios. Sec. III will compare the four derated conditions in terms of performance indicators. Last, Sec. IV will summarize the findings and the conclusions of the analysis.

## II. Multi-Three-Phase Motor Modeling

According to the literature, M3PH machines can be modeled using different approaches. This paper considers the multi-stator (MS) one since it models the machine as multiple three-phase winding sets operating in parallel and interacting with the rotor. This way, the flux and torque contributions of

TABLE I
PM-SyR Machine Ratings

| | | |
|---|---|---|
| Rated power | (kW) | 60 |
| Peak torque | (Nm) | 950 |
| Rated speed | (rpm) | 1000 |
| Maximum speed | (rpm) | 3000 |
| DC-link voltage | (V) | 600 |
| Rated phase current | (Apk) | 34 |
| Peak phase current | (Apk) | 50 |
| Stator outer diameter | (mm) | 375 |
| Rotor outer diameter | (mm) | 238 |
| Airgap length | (mm) | 1 |
| Stack length | (mm) | 340 |
| Number of phases | | 14 (4x3phase) |
| Number of pole pairs | | 2 |
| Number of stator slots | | 48 |
| Winding configuration | | Asymmetrical, full pitch |
| Turns in series per phase | | 46 |

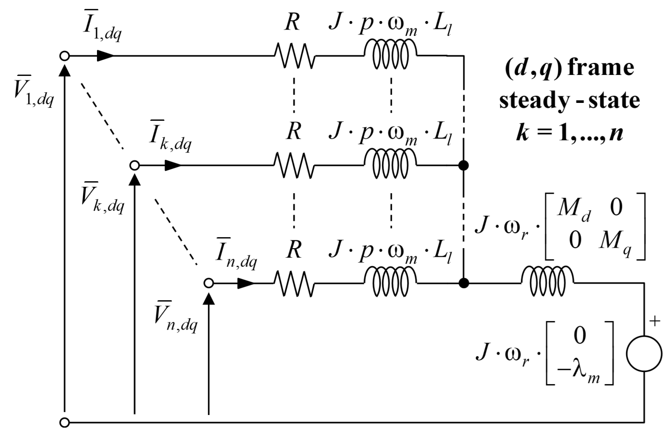


Fig. 2. MS-based steady-state equivalent circuit of a M3PH PM-SyR.

each three-phase winding set are highlighted, preserving the modularity feature at the modeling level. Therefore, based on the MS modeling [11], an M3PH PM-SyR motor presenting $n$ three-phase winding sets can be modeled using $n$ equation systems. Considering the generic three-phase winding set $k$ ($k = 1, \ldots, n$), the dq voltage equations are expressed as:

$$\bar{v}_{k,dq} = R \cdot \bar{i}_{k,dq} + \frac{d}{dt}\bar{\lambda}_{k,dq} + p \cdot \omega_m \cdot J \cdot \bar{\lambda}_{k,dq} \tag{1}$$

where $\bar{x}_{k,dq} = [x_{k,d} x_{k,q}]^t$ are the $k$-set stator vectors of voltage $v$, current $i$, and flux linkage $\lambda$, while $J$ is the matrix-form complex operator. In (1), it is reasonably assumed that the three-phase winding sets exhibit the same stator resistance value $R$. Like for the 3PH motors, the back-emf contributions are modulated by the electric speed of the motor computed as pole pair p times the mechanical one $\omega_m$. Regarding the current-to-flux model of the machine, each generic three-phase winding set $k$ ($k = 1, \ldots, n$) is ruled by the following $dq$ current equations:

$$\bar{\lambda}_{k,dq} = L_l \cdot \bar{i}_{k,dq} + \begin{bmatrix} M_d & 0 \\ 0 & M_q \end{bmatrix} \cdot \sum_{z=1}^{n} \bar{i}_{z,dq} - \begin{bmatrix} 0 \\ \lambda_m \end{bmatrix} \tag{2}$$

where $M_d$ and $M_q$ are the magnetizing $dq$ inductances, while $\lambda_m$ is the PM flux linkage aligned with the negative $q$-axis according to the SyR motor convention. Similarly to the resistance, it is reasonably assumed that the three-phase winding sets also exhibit the same leakage inductance value $L_l$. It is noted that the magnetizing flux of the machine depends on the sum of the $dq$ currents of the three-phase winding sets regardless of whether these operate balanced or not. This behaviour is well-evident from the MS-based steady-state equivalent circuit of the M3PH PM-SyR motor shown in Fig. 2 [11]. Finally, according to the machine's power balance, the overall torque T is given by the contributions sum of the three-phase winding sets as in (3).

$$T = \frac{3}{2} \cdot p \cdot \sum_{k=1}^{n} (\lambda_{k,d} \cdot i_{k,q} - \lambda_{k,q} \cdot i_{k,d}) \tag{3}$$

In this paper, the analysis of the machine performance in normal and open-three-phase fault conditions is executed by considering a balanced operation between the three-phase winding sets. Indeed, this condition corresponds to the maximum torque production efficiency [12]. Therefore, considering any of the active three-phase winding sets, (1) and (2) are simplified as:

$$\begin{cases} \bar{v}_{dq} = R \cdot \bar{i}_{dq} + \frac{d}{dt}\bar{\lambda}_{dq} + p \cdot \omega_m \cdot J \cdot \bar{\lambda}_{dq} \\ \bar{\lambda}_{dq} = L_l \cdot \bar{i}_{dq} + \begin{bmatrix} M_d & 0 \\ 0 & M_q \end{bmatrix} \cdot n_{active} \cdot \bar{i}_{dq} - \begin{bmatrix} 0 \\ \lambda_m \end{bmatrix} \end{cases} \tag{4}$$

where $n_{active}$ stands for the number of active three-phase winding sets. It is noted that subscript $k$ is missing in (4). Indeed, if the three-phase winding sets operate balanced with each other, there is no difference between their $dq$ voltages, $dq$ currents, and $dq$ flux linkages. Similarly to the voltage and current equations, the overall torque equation (3) is simplified as follows.

$$T = \frac{3}{2} \cdot p \cdot n_{active} \left(\lambda_d \cdot i_q - \lambda_q \cdot i_d\right) \tag{5}$$

Based on (4) and (5), the machine's maps (flux linkages, torque, losses) in balanced conditions among the active three-phase winding sets can be thus straightforwardly expressed in terms of overall $dq$ currents using the MS modeling, i.e., adopting $(n_{active} \cdot i_d, n_{active} \cdot i_q)$ as reference axes hereafter.

## III. Derated Magnetic Model Assessment

In the following, the magnetic model (i.e. flux linkage, torque and loss maps) will be compared for the derated scenarios. Each configuration is expressed by a binary vector, representing the four three-phase sets of the motor. For instance, the configuration [1 1 1 1] identify the healthy condition (all the sets active), while in the configuration [1 1 0 0], sets 1 and 2 are active, while sets 3 and 4 are disconnected. The 5 considered scenarios are:

- **[1 1 1 1]**: healthy condition, all units active;
- **[1 1 1 0]**: light derating condition, just one set inactive;
- **[1 1 0 0]**: average derating condition, two adjacent sets active;
- **[1 0 1 0]**: average derating condition, two alternated sets active;
- **[1 0 0 0]**: severe derating condition, just one set active.

Please, note that in the listed scenarios, set 1 is always active, but the considered scenario is valid for all the similar conditions. For instance, scenario [1 0 1 0] and scenario [0 1 0 1] are the same on the magnetic point of view, assuming that the sets are balanced.

### A. Flux Linkage and Torque Maps

The flux maps are FEA computed for all the considered scenarios and reported in Fig. 3. All the maps are computed up to the maximum phase current allowed by the units inverter. It is worth noting that, on a fundamental point of view, the derating act in a linear way: halving the current loading will half the flux linkage in the motor, without additional effects on saturation and cross saturation. Indeed, the flux linkage contours, both for $d$ and $q$ axis are almost perfectly superimposed for each considered scenario, with the only difference of the current limit.

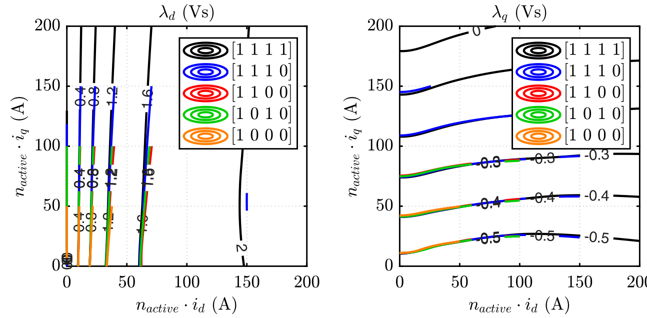


(a) (b)

Fig. 3. Flux linkage maps comparison for the selected derating scenarios: a) $d$ axis flux linkage and b) $q$ axis flux linkage.

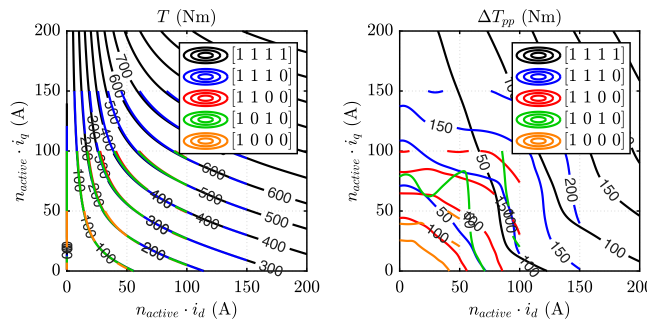


(a) (b)

Fig. 4. Flux linkage maps comparison for the selected derating scenarios: a) average torque map and b) peak-to-peak torque ripple map.

From the same FEA identification, the torque and torque ripple maps can be retrieved and are reported in Fig. 4. In details, the average torque and the peak-to-peak torque ripple maps are considered. Dealing with the average torque, the comments done for fundamental flux maps hold. Indeed, the torque contours are almost perfectly superimposed for all the considered faulted scenarios, with the only limits dictated by the maximum current limit. The comparison for toque ripple is drastically different. Indeed, the torque ripple contours present different shapes and values, function of the considered scenario. This difference is mainly caused by the different harmonic content that the derated conditions induce, as will be demonstrated later. It is worth noting that the healthy condition is the one expressing lower torque ripple, while the asymmetric fault conditions (namely [1 0 0 0], [1 1 0 0] and [1 0 0 0]) presents drastically higher torque ripple values, as will be clarified later.

The peak-to-peak torque ripple maps are compared in details in Fig. 5. There, the derated scenarios are reported with colored

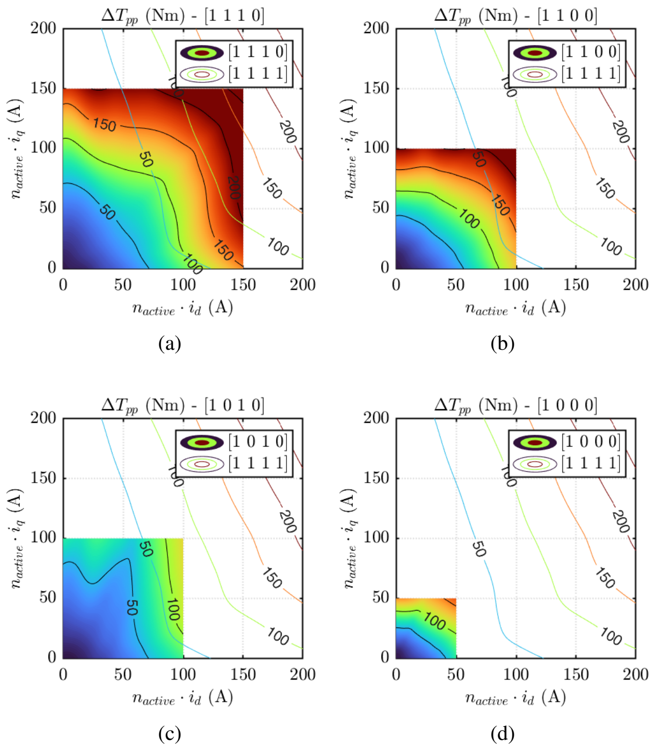


Fig. 5. Peak-to-peak torque ripple maps of derated condition and comparison with the healthy condition.

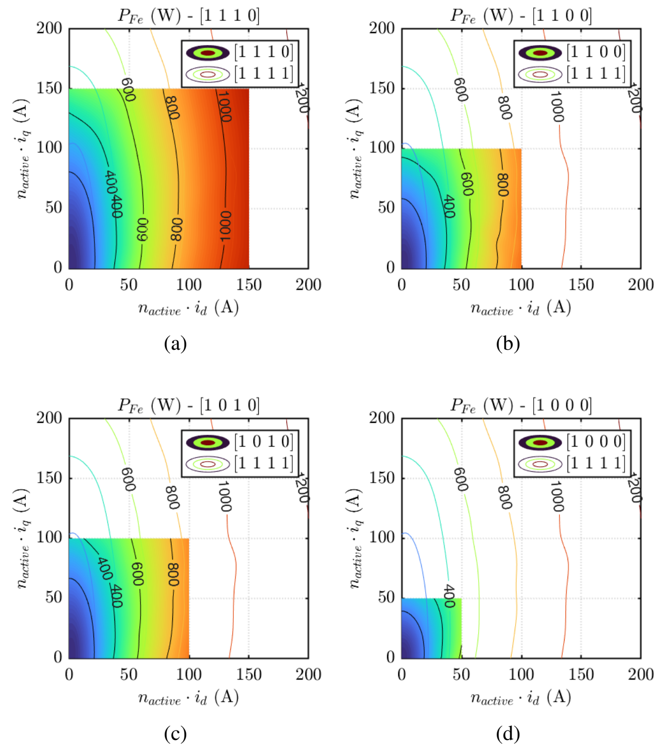


Fig. 6. Iron loss maps of derated condition and comparison with the healthy condition.

map, while the healthy condition is reported with colored lines. In this format, the difference between the derated conditions in evident. If asymmetric deratings are performed ([1 1 1 0], [1 1 0 0] and [1 0 0 0]), the torque ripple drastically increase, with a factor of more than 2, compared to the 4 units condition. On the other hand, the configuration [1 0 1 0] is the configuration that presents the lowest torque ripple degradation, mainly because of the symmetry of its configuration and values that are also half of the condition [1 1 0 0].

### *B. Iron Loss Maps*

The iron loss are mapped over the $(i_d, i_q)$ domain at constant speed, with a procedure similar for the flux maps identification, as reported in [9]. The identification is repeated for each considered scenario and the results are compared in Fig. 6. Also in this case, the four derated conditions are reported with shaded contours, while the full set condition is reported with colored contours. The difference in derating is more pronounced than the torque and flux linkage, but not critical as for torque ripple. In general, the rotor loss are the one that suffer more from the additional induced harmonic content, however, the majority of iron loss are localized at the stator core, reducing the impact of additional harmonic on the iron loss. Indeed, the main differences between full sets and derated condition on iron loss are visible for low $d$ axis current and high $q$ axis current, where the flux linkage is aligned along the $q$ axis and the rotor slotting effect is more pronounced.

### *C. Operating Point Comparison*

The maps on the $(i_d, i_q)$ domain presented before can give good idea of the general output of the motor for different operative conditions. However, to have a deeper understanding of the differences, the MTPA condition at 1/4 of the maximum current loading is considered and verified in details. This condition represents the peak condition if just one set is active and partial loads if multiple sets are enabled and is selected because all the configuration can run in this conditions. Fig. 7 reports the torque waveform for the 5 conditions and the respective FFT. Besides the waveform, that show the different harmonic content but are difficult to read, the important result is the FFT bar chart. Here problems of having unbalanced open set is evident, since all the harmonics multiple of 6 are visible. As expected, for the healthy condition, the first torque ripple harmonic is the $24^{th}$, while the scenario [1 0 1 0] is equivalent to an asymmetric six phase configuration, with the main torque ripple harmonic equal to 12. This is the main reason of the better torque ripple and loss behavior of this configuration, among all the derated scenarios.

The analysis is expanded also to the flux linkage waveform and its harmonic content (currents are sinusoidal in this analysis). To have a better and more complete understanding, the magnetizing flux linkage is computed for each condition and rotor position, by integrating the airgap flux density. In this way, also additional leakage flux linkage can be detected and the effect of unbalanced units distribution on

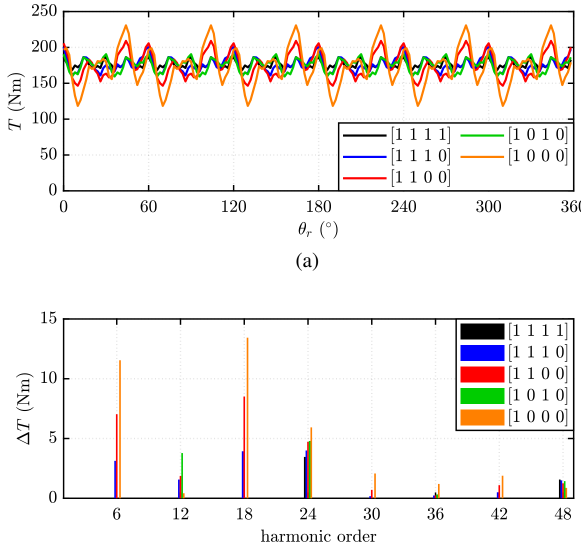


(b)

Fig. 7. Details on the selected operating point for the 5 scenarios: a) torque waveform function of the rotor position and b) torque ripple FFT.

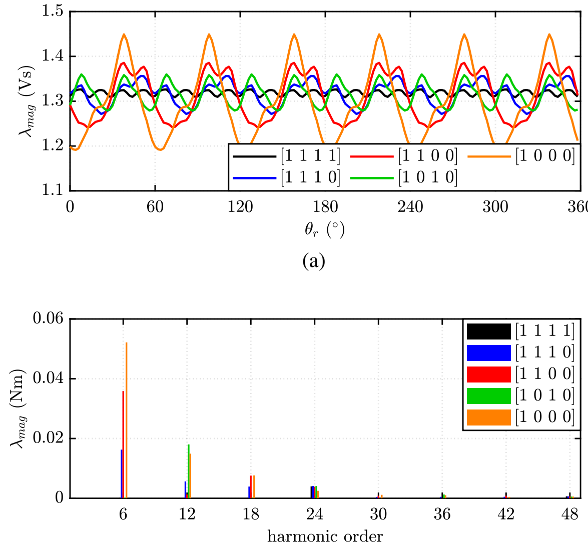


(b)

Fig. 8. Details on the selected operating point for the 5 scenarios: a) magnetizing flux linkage waveform function of the rotor position and b) its FFT.

the istantaneous zero-sequence flux linkage is identified. The results are reported in Fig. 8. Here the effect of the open units on the waveform is more evident, while the harmonic content is aligned with the torque ripple FFT. For the unbalanced conditions, the amplitude of the critical harmonic is way higher than the balanced situations, given that the fundamental value is the same for all the configurations.

A last comparison on this operating condition is done at the flux density distribution level. In this comparison, the harmonic content highlighted in Fig. 8 is not visible, since a single rotor position is considered, however, the leakage paths with derated supply are visible. The results are shown in Fig. 9, with the active winding colored in blue and unactive winding colored in red. The better flux density distribution of configuration [1 1 1 1] is clearly visible, while the other motors presents oversaturated stator teeth. Furthermore, among the half derating configurations, [1 0 1 0] presents the most distributed stator iron saturation. Last, here is clearly visible also the effect of mutual coupling between the sets, with most of the flux linkage created by the active units that is seen also from the inactive sets.

## IV. Derated Performance Figures Assessment

Once the flux and loss maps are computed, the performance figures of the motor in each scenario can be retrieved by flux and loss maps elaboration [9].

### A. Control Trajectories

A first comparison between the five conditions is the torque and torque ripple characteristics along the Maximum Torque per Ampere (MTPA) trajectory. As the torque map is almost the same for the healthy and derated conditions, the MTPA trajectory is the same for all the case. Fig. 10 reports the torque versus current and the torque ripple versus torque curves for the healthy case (black line) and the derated conditions (colored lines). The findings highlighted in the previous section are confirmed, but a better quantification on the differences can be done in this framework. First of all, the average torque is function of the total current loading and just slightly affected by how the current is distributed among the units. This is a simple but important point, and support the fact that partial load can be obtained theoretically with some units turned off. However, this conclusion neglects the harmonic content in derating operations. Dealing with torque ripple, the best condition is to have all the sets enabled, as highlighted

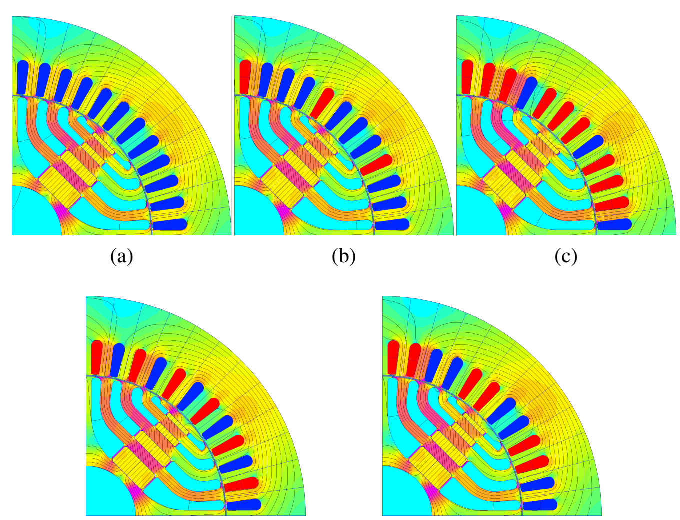


(e)

Fig. 9. Flux density distribution at MTPA and 1/4 of the maximum current loading: a) [1 1 1 1], b) [1 1 1 0], c) [1 0 0 0], d) [1 0 1 0] and e) [1 1 0 0]

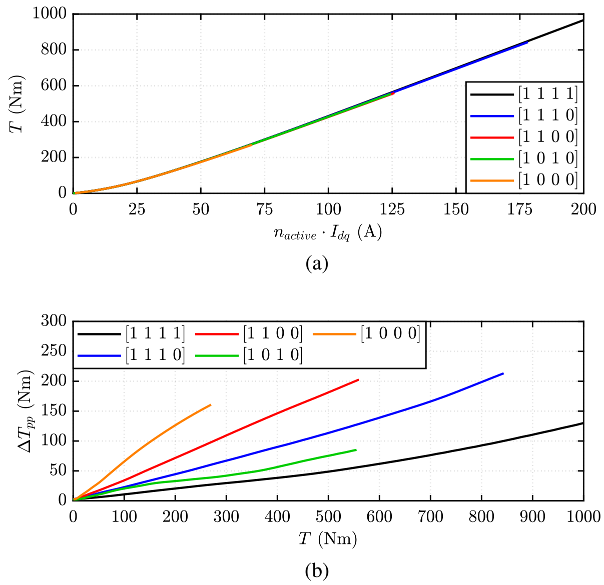


Fig. 10. MTPA curves comparison: a) torque versus current characteristic, b) peak-to-peak torque ripple versus torque curves.

previously. As some sets are turned off, the harmonic content increase and torque ripple worsen. For instance, for heavy derating conditions (output torque lower than 1/4 of the rated torque), the [1 1 1 1] condition is still superior than the derated condition [1 0 0 0], that presents a torque ripple more than 3 times higher. Another interesting point is the comparison between the two medium derating conditions, [1 1 0 0] and [1 0 1 0]. Even if the torque-current relation is the same, the torque ripple for the [1 1 0 0] scenario is almost twice than [1 0 1 0], that is still slightly higher than the full set configuration. This difference is related to the more uniform flux density distribution of the second configuration, compared to the former, that mimic quite well the behavior of the healthy supply.

### B. *Efficiency Maps*

One of the most important metrics for electrical machines is the efficiency map. The maps are retrieved from flux and loss maps for all the scenarios with the method presented in [9] and extended for N3PH machines. The results are reported and compared in Fig. 11. As expected, the main effect of disabling units is the reduction of maximum torque and the torque limit at each considered speed. Furthermore, the efficiency is slightly reduced when units are turned off. This is mainly caused by additional iron loss, since the flux maps are practically independent from the number of active units. Dealing with the half derating condition, the balanced configuration ([1 0 1 0]) presents slightly higher efficiency than the asymmetric configuration, because of the lower harmonic content. When system efficiency considerations are studied, the way of turning off the units must be considered, even at efficiency level and not just at torque ripple level.

### C. *Torque Ripple Maps*

From the same analysis, other metrics can be extracted, since the adopted procedure compute all the loss terms and the $(i_d, i_q)$ tables for the control. Among all the possible metrics, here the focus is set on the torque ripple, because of the tight link with the harmonic. The peak-to-peak torque ripple over the $(T, n)$ domain is reported in Fig. 12 for the 5 scenarios. Unlike for efficiency maps, torque ripple presents deep differences among the supply type, as highlighted previously. The healthy condition is not critical, since torque ripple reach about 12% below base speed and is even lower in field weakening condition. About the derated conditions, the torque ripple is quite higher, as expected from the previous analysis. Contrary from the healthy condition, the torque ripple is not mitigated in field-weakening condition and the values are in general higher. Remarkable is the difference between [1 1 0 0] and [1 0 1 0] configuration: the advantage in term of torque ripple and harmonic content in general of the latter is valid for the whole torque-speed domain. Furthermore, the [1 0 1 0] configuration presents the lowest toque ripple among the derated scenarios. This suggest that, if the application is quite sensitive to torque ripple, in case of fault on one unit, the [1 0 1 0] configuration can be implemented, allowing non-critical torque undulation with halved performance.

## V. Conclusion

The paper studied the performance derating of M3PH machines with high number of units. The analysis focus on a 12 phase machine (4x3 phase sets) with asymmetric winding and high coupling between the sets and consider all the possible open-three-phase conditions. The analysis confirms that the performance metrics based on fundamental quantities are independent on the number of active units, given that the current loading condition if fulfilled. Indeed, average torque and maximum torque per speed limit can be defined independently from the number of active units (given the unit current limit). On the other side, the performance indexes based on harmonic content are heavily affected by the number of active units and which are the active units. In general, the loss of three-phase units cause an increase in harmonic content, that reflects in higher torque ripple and iron loss. However, it is also highlighted that a derated condition which maintains the balanced distribution of the current density in the slots can reduce the harmonic content, having just a slight detriment compared to the healthy condition. Thermal and HVH indexes are neglected in this analysis but can affect the preferred strategy in case of loss on one units, eventually suggesting to turn off another healthy units, in order to achieve reduced torque undulation and avoiding possible mechanical damages.

## Acknowledgment

The research has been conducted with the support of Power Electronics Innovation Center (PEIC) of Politecnico di Torino.

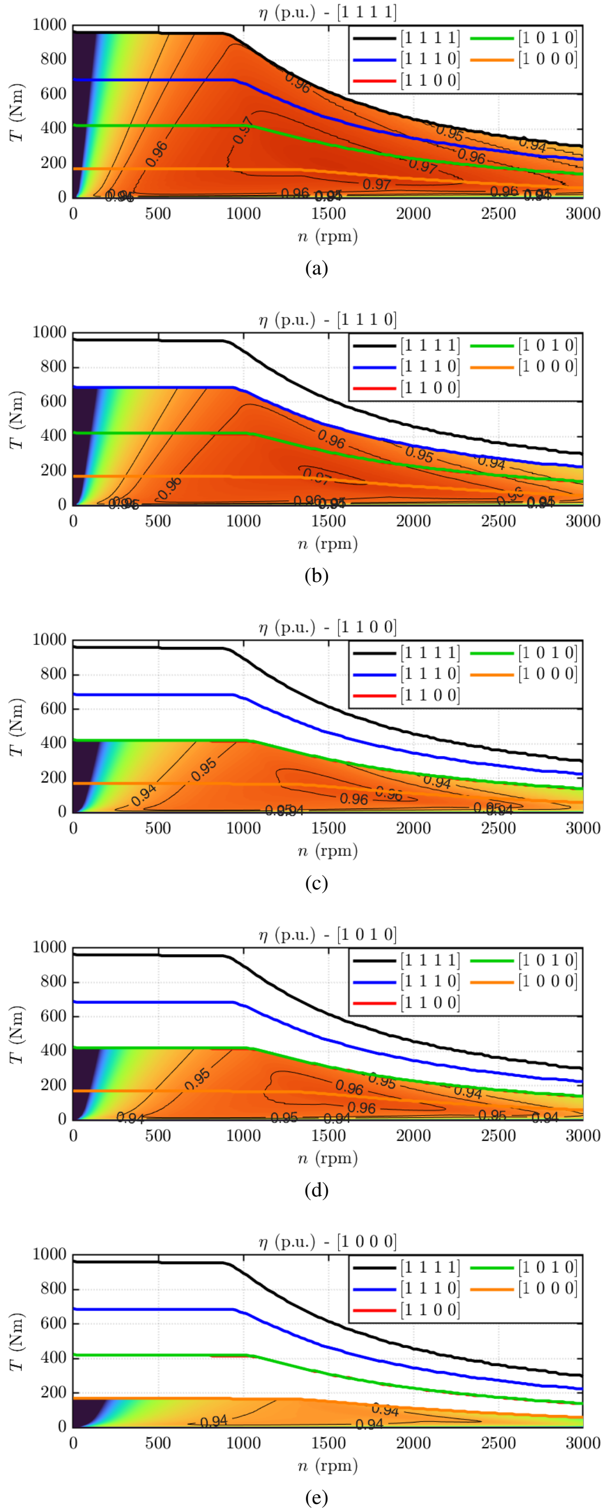


Fig. 11. Efficiency maps of the 5 considered scenarios at rated voltage and maximum current.

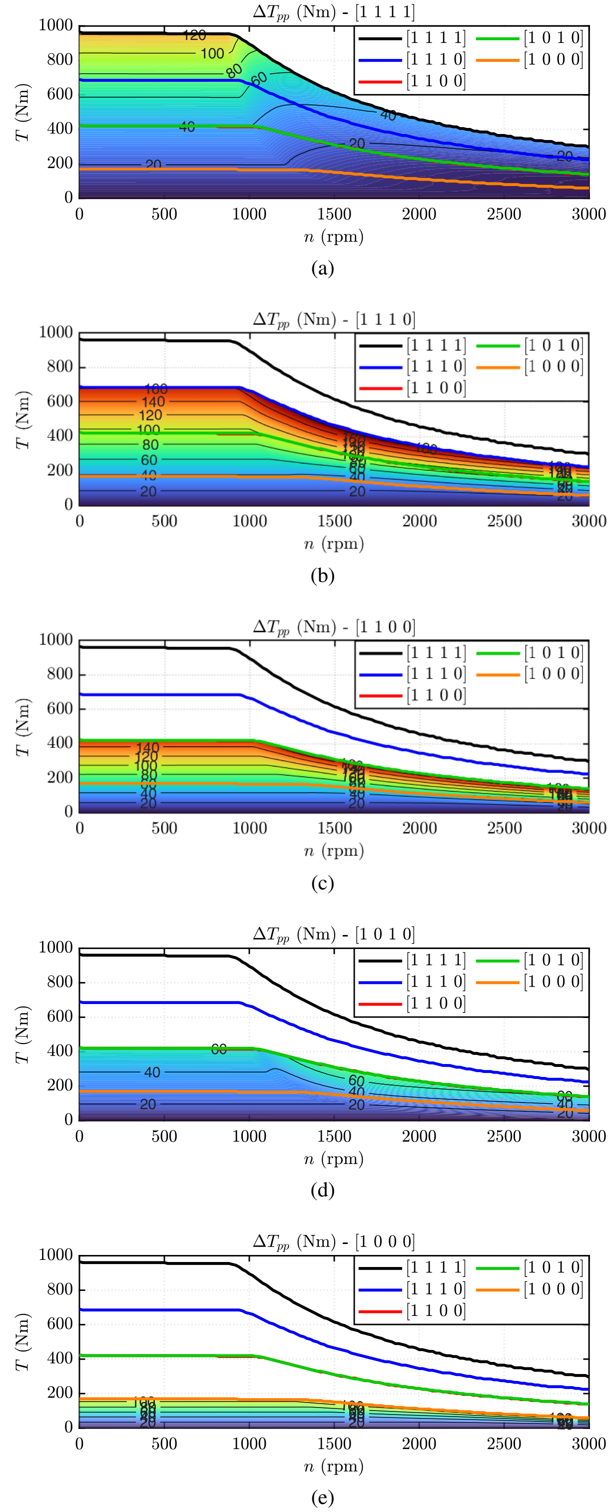


Fig. 12. Peak-to-peak torque ripple maps over the torque-speed plane of the 5 considered scenarios at rated voltage and maximum current.

## REFERENCES


[1] A. Salem and M. Narimani, "A review on multiphase drives for automotive traction applications," *IEEE Transactions on Transportation Electrification*, vol. 5, no. 4, pp. 1329–1348, 2019.

[2] R. Bojoi, S. Rubino, A. Tenconi, and S. Vaschetto, "Multiphase electrical machines and drives: A viable solution for energy generation and transportation electrification," in *2016 International Conference and Exposition on Electrical and Power Engineering (EPE)*, 2016, pp. 632–639.

[3] C. Babetto, N. Bianchi, A. Torreggiani, C. Bianchini, M. Davoli, and A. Bellini, "Design Optimization and Analysis of a Synchronous

Reluctance Machine for Fault-Tolerant Applications," in *2019 IEEE International Electric Machines & Drives Conference (IEMDC)*. San Diego, CA, USA: IEEE, May 2019, pp. 1784–1791. [Online]. Available: https://ieeexplore.ieee.org/document/8785107/

[4] C. Tong, F. Wu, P. Zheng, Y. Sui, and L. Cheng, "Analysis and design of a fault-tolerant six-phase permanent-magnet synchronous machine for electric vehicles," in *2014 17th International Conference on Electrical Machines and Systems (ICEMS)*. Hangzhou, China: IEEE, Oct. 2014, pp. 1629–1632. [Online]. Available: http://ieeexplore.ieee.org/document/7013738/

[5] B. Wang, Y. Liu, G. Vakil, T. Yang, and Z. Zhang, "Feasibility of Permanent Magnet Fault Tolerant Machines for Aircraft Starter/Generator Systems," in *2020 International Conference on Electrical Machines (ICEM)*. Gothenburg, Sweden: IEEE, Aug. 2020, pp. 2104–2110. [Online]. Available: https://ieeexplore.ieee.org/document/9270965/

[6] A. Akay and P. Lefley, "Research on torque ripple under healthy and open-circuit fault-tolerant conditions in a PM multiphase machine," *CES Transactions on Electrical Machines and Systems*, vol. 4, no. 4, pp. 349–359, Dec. 2020. [Online]. Available: https://ieeexplore.ieee.org/document/9312764/

[7] K. Nounou, J. F. Charpentier, K. Marouani, M. Benbouzid, and A. Kheloui, "Emulation of an electric naval propulsion system based on a multiphase machine under healthy and faulty operating conditions," *IEEE Transactions on Vehicular Technology*, vol. 67, no. 8, pp. 6895–6905, 2018.

[8] A. T. Abdel-Wahed, M. Y. Metwly, A. Hemeida, A. S. Abdel-Khalik, M. S. Hamad, and S. Ahmed, "Performance comparison of six-phase pm machine with several winding layouts for ev applications," in *2023 IEEE Conference on Power Electronics and Renewable Energy (CPERE)*, 2023, pp. 1–7.

[9] S. Ferrari, P. Ragazzo, G. Dilevrano, and G. Pellegrino, "Flux and loss map based evaluation of the efficiency map of synchronous machines," *IEEE Transactions on Industry Applications*, vol. 59, no. 2, pp. 1500–1509, 2023.

[10] S. Ferrari and G. Pellegrino, "SyR-e: Synchronous Reluctance (machines) - evolution." [Online]. Available: www.github.com/SyR-e

[11] S. Rubino, O. Dordevic, R. Bojoi, and E. Levi, "Modular vector control of multi-three-phase permanent magnet synchronous motors," *IEEE Transactions on Industrial Electronics*, vol. 68, no. 10, pp. 9136–9147, 2021.

[12] I. Zoric, M. Jones, and E. Levi, "Arbitrary power sharing among three-phase winding sets of multiphase machines," *IEEE Transactions on Industrial Electronics*, vol. 65, no. 2, pp. 1128–1139, 2018.